

Enhanced detection of myeloperoxidase activity in deep tissues through luminescent excitation of near-infrared nanoparticles

Ning Zhang^{1,3}, Kevin P Francis¹, Arun Prakash² & Daniel Ansaldi¹

A previous study reported the use of luminol for the detection of myeloperoxidase (MPO) activity using optical imaging in infiltrating neutrophils under inflammatory disease conditions. The detection is based on a photon-emitting reaction between luminol and an MPO metabolite. Because of tissue absorption and scattering, however, luminol-emitted blue light can be efficiently detected from superficial inflammatory foci only. In this study we report a chemiluminescence resonance energy transfer (CRET) methodology in which luminol-generated blue light excites nanoparticles to emit light in the near-infrared spectral range, resulting in remarkable improvement of MPO detectability *in vivo*. CRET caused a 37-fold increase in luminescence emission over luminol alone in detecting MPO activity in lung tissues after lipopolysaccharide challenge. We demonstrated a dependence of the chemiluminescent signal on MPO activity using MPO-deficient mice. In addition, co-administration of 4-aminobenzoic acid hydrazide (4-ABAH), an irreversible inhibitor of MPO, significantly attenuated luminescent emission from inflamed lungs. Inhibition of nitric oxide synthase with a nonspecific inhibitor, L-NAME, had no effect on luminol-mediated chemiluminescence production. Pretreatment of mice with MLN120B, a selective inhibitor of IKK-2, resulted in suppression of neutrophil infiltration to the lung tissues and reduction of MPO activity. We also demonstrated that CRET can effectively detect MPO activity at deep tissue tumor foci due to tumor development-associated neutrophil infiltration. We developed a sensitive MPO detection methodology that provides a means for visualizing and quantifying oxidative stress in deep tissue. This method is amenable to rapid evaluation of anti-inflammatory agents in animal models.

MPO is a heme-containing enzyme that is abundant in neutrophils and macrophages and functions as a key mediator of the phagocytic oxidative burst and inflammatory process¹. MPO catalyzes the conversion of hydrogen peroxide and chloride ions into hypochlorous acid, which is one of the most reactive oxidants produced *in vivo*². Hypochlorous acid oxidizes lipids, proteins and DNA and

thus promotes tissue injury and inflammation³ during the pathological progress of chronic obstructive pulmonary disease⁴ (COPD) and atherosclerosis⁵. Circulating concentrations of MPO have been shown to predict risk for major adverse cardiac events. In addition, amounts of MPO-derived chlorinated compounds have been used as specific biomarkers for disease progression⁶. There has been considerable interest in the development of therapeutically useful MPO inhibitors. A previous study showed that 4-ABAH irreversibly inhibits hypochlorous acid production as a suicide substrate of MPO⁷. A means of monitoring MPO activity under *in vivo* conditions should help establish the relationship between MPO induction and pathological progression and facilitate preclinical evaluation of MPO inhibitors.

Noninvasive imaging of MPO enzymatic activity with luminol was previously reported⁸. These researchers found that luminol specifically interacts with hypochlorous acid to produce an emission of luminescent light that can be detected through optical imaging. When we applied luminol to several inflammatory disease models, we found that the detection was the most sensitive for superficially located inflammatory foci but was much less sensitive, and was undetectable in many cases, for deep tissue inflammation. A lack of sensitivity for the detection of deep tissue inflammation is the result of the poor penetration capability of luminol-emitted short-wavelength light ($\lambda_{\text{max}} = 425 \text{ nm}$) through animal tissues. It is well established that photons in the near-infrared (NIR) region (particularly 700–900 nm) are more penetrative through animal tissues because of reduced absorption and scattering⁹. We questioned whether NIR nanoparticles could be used to red shift luminol-emitted blue light to NIR, thus improving the *in vivo* detectability of MPO.

Previous work has established that luciferase or horseradish peroxidase conjugated to quantum dots allows luminescence to be absorbed and re-emitted by the nanoparticles, a phenomenon known as bioluminescence resonance energy transfer¹⁰ (BRET) or CRET¹¹. We hypothesized that luminescence energy transfer may also occur when the fluorescence acceptor is in a nonconjugated state. We tested this hypothesis by administering Luminol-R, a mixture of luminol and near-infrared quantum dots, to mice with induced lung inflammation or metastatic cancer. We demonstrate that luminol-emitted

¹Caliper Life Sciences, Alameda, California, USA. ²Department of Anesthesia and Perioperative Care, San Francisco General Hospital, University of California, San Francisco, California, USA. ³Present address: *In Vivo* Pharmacology and Oncology, Pharmaron, Beijing, China. Correspondence should be addressed to N.Z. (ning.zhang@pharmaron.com).

Received 17 October 2011; accepted 20 September 2012; published online 3 March 2013; doi:10.1038/nm.3110

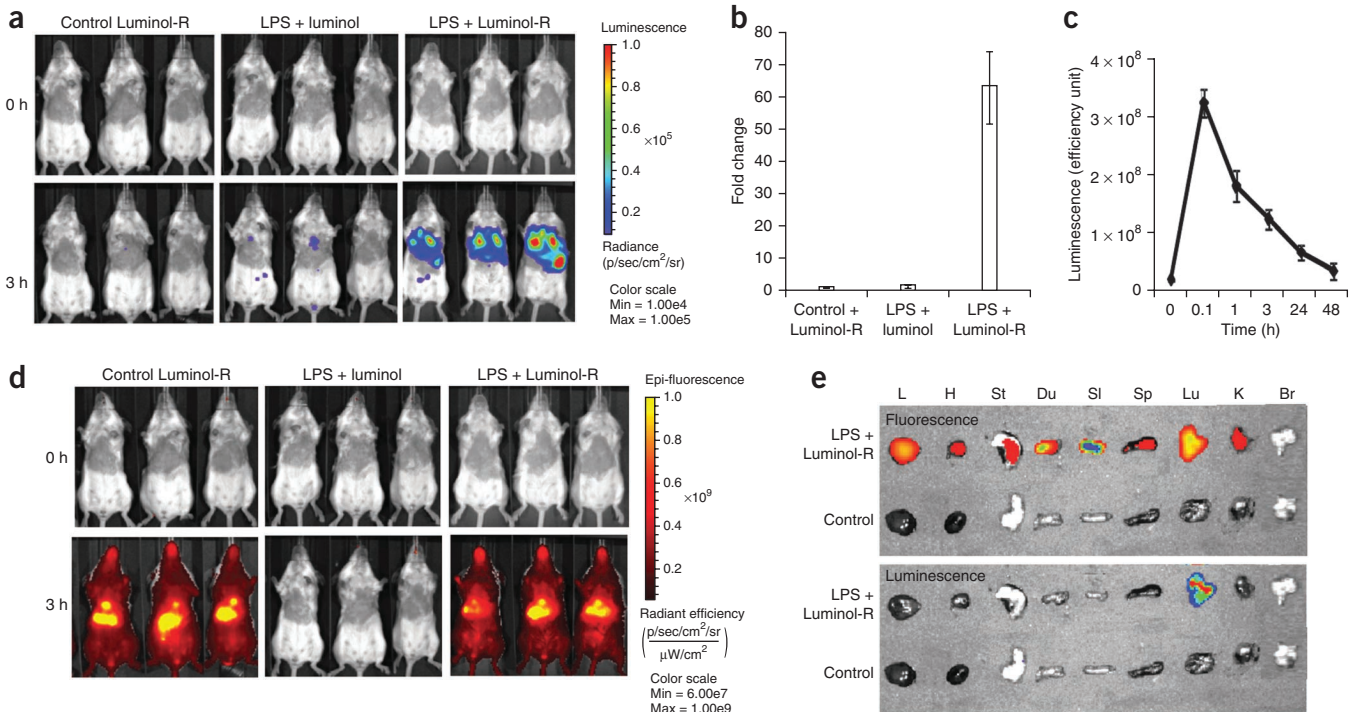


Figure 1 Detection of pulmonary inflammation with Luminol-R. **(a-d)** Luminescent and fluorescent signals detected in BALB/CJ mice intratracheally delivered with LPS or PBS (control) and then i.v. injected with Luminol-R or luminol 3 h later. Shown are luminescent (**a**) and fluorescent (**d**) images detected with an IVIS Spectrum instrument, as well as quantifications of the luminescent signals from the lungs (**b,c**). Data are presented as the mean \pm s.e.m. ($n = 4$ per group). **(e)** Ex vivo analysis of liver (L), heart (H), stomach (St), duodenum (Du), small intestine (SI), spleen (Sp), lungs (Lu), kidney (K) and brain (Br) performed with fluorescent imaging (excitation at 745 nm and emission at 800 nm) and luminescent imaging.

short-wavelength light can be red shifted by quantum dots through CRET, resulting in an increase in MPO detectability from deep-seated inflammatory foci. We show the utility of Luminol-R as a luminescent MPO readout and for evaluation of MPO inhibition under both *in vitro* and *in vivo* conditions.

RESULTS

Enhanced detection of MPO activity with quantum dots

To test whether quantum dots can be used to red shift luminol-emitted blue light, we concomitantly administered luminol and 800-nm-emitting quantum dots (Luminol-R) to mice with induced MPO activity. We selected a lipopolysaccharide (LPS)-induced pulmonary inflammation model because of previous difficulty in using luminol to detect MPO activity in lung tissues. We intravenously (i.v.) injected Luminol-R into mice at 3 h after LPS delivery and then imaged the mice for luminescent signals (Fig. 1a,b). As compared to luminol-injected mice that had relatively low-level luminescent signals ($1.15 \times 10^3 \pm 0.78 \times 10^3$ (mean \pm s.e.m) photons $\text{cm}^{-2} \text{sr}^{-1} \text{s}^{-1}$), mice receiving Luminol-R showed robust luminescent signals ($42.4 \times 10^3 \pm 15 \times 10^3$ photons $\text{cm}^{-2} \text{sr}^{-1} \text{s}^{-1}$) in the lungs. MPO detection by Luminol-R was 37-fold more sensitive than detection by luminol. Longitudinal imaging showed that Luminol-R-emitted luminescence reached its peak at 20 min and gradually declined to a basal level by 180 min (Fig. 1c).

We also monitored the distribution of quantum dots with fluorescent imaging (Fig. 1d). Quantum dot-mediated fluorescence was distributed throughout the body. Ex vivo imaging detected fluorescence in the liver, heart, stomach, duodenum, small intestine, spleen, lungs and kidney tissues but not in brain tissue, indicating that quantum

dots did not cross the blood-brain barrier. Luminol-R-emitted luminescence was only detectable in the lungs (Fig. 1e).

CRET improved *in vivo* detectability of MPO activity

To determine whether CRET occurred with quantum dots in a nonconjugated state, we set up *in vitro* MPO reactions with and without quantum dots and spectrally analyzed the reactions. The MPO reaction with luminol alone produced a luminescence emission peak at 425 nm (Fig. 2a). In the presence of quantum dots 800, a new luminescence peak at 800 nm was detectable in a quantum dot concentration-dependent fashion, supporting our hypothesis that luminescence energy transfer occurs when the fluorescence acceptor is in a nonconjugated state. CRET also occurred under *in vivo* conditions. We observed three emission peaks at 445 nm, 625 nm and 800 nm in freshly resected lungs taken from LPS-challenged mice (Fig. 2b). The 800-nm peak, which comprised 13% of the total luminescent signals emitted from Luminol-R, is the expected emission spectrum of 800-nm-emitting quantum dots. The 625-nm peak was caused by tissue absorption and re-emission of the luminol signal, as it was missing from the *in vitro* MPO spectral analysis assay.

We also analyzed the emission spectrum under *in vivo* conditions with an IVIS Spectrum imaging system, which showed that the CRET signal comprised 81% of the total detectable luminescence (Fig. 2c). When compared with *ex vivo* imaging that detected strong luminescent signals, *in vivo* imaging detected only ~7% of the luminescence measured *ex vivo* (Fig. 2d). These results indicate that *in vivo* detection of the luminol-emitted light is dependent predominantly on the red-shifted CRET signal.

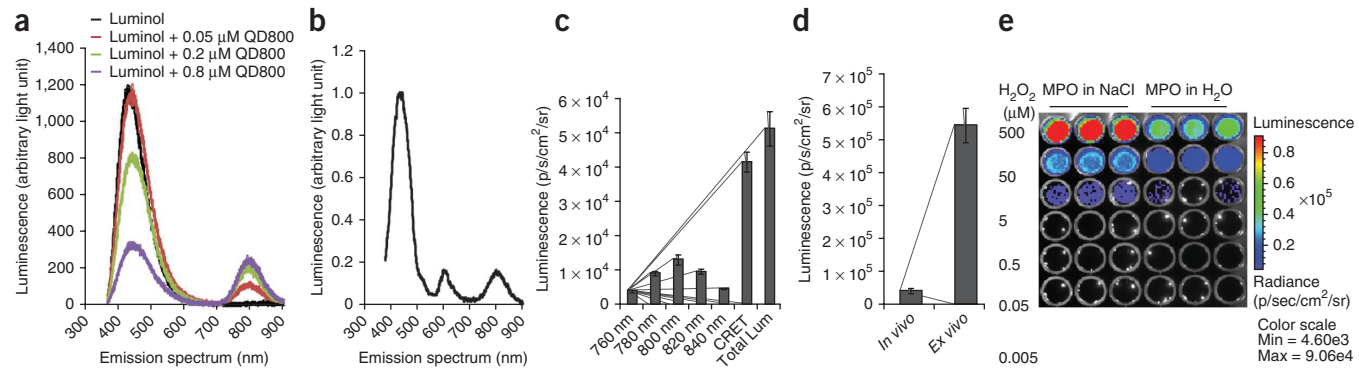


Figure 2 Confirmation that CRET substantially improves the *in vivo* detectability of MPO activity. (a) MPO and Luminol-R assay mix analyzed with a TRIAX 320 spectrometer. QD800, quantum dots emitting at 800 nm. (b,c) *Ex vivo* spectral analyses of freshly resected lungs from LPS-challenged mice with a TRIAX 320 spectrometer (b) and an IVIS Spectrum instrument (c). CRET, the cumulative red-shifted luminescent signals from the lungs; total Lum, all the luminescent signals collected with an open filter. (d) Comparison of the luminescent signals from the lungs measured *in vivo* and *ex vivo*. (e,f) The effect of MPO assay, set up as above but with hydrogen peroxide added to the indicated final concentrations, analyzed with an IVIS Spectrum instrument. BLI, bioluminescence imaging. (g) MPO and LPO assays analyzed with an IVIS Spectrum instrument. Data are shown as the mean luminescent signals \pm s.e.m. (c,d,f,g). $n = 3$ per group.

Peroxidase and chlorination activities of MPO

It is well known that MPO shows chlorination and peroxidation activity as a result of activation by hydrogen peroxide. We designed an experiment to dissect the contribution of these activities with respect to luminescent production by MPO. We found much stronger luminescent signals in MPO reactions that contained both sodium chloride and hydrogen peroxide in a manner that was dependent on the concentration of hydrogen peroxide (Fig. 2e). At hydrogen peroxide concentrations of 500 μ M and 50 μ M, the luminescent emissions of the MPO reactions without sodium chloride were 35% and 49%, respectively, compared to the identical reactions with sodium chloride, indicating that chlorination dominated over peroxidation under these conditions (Fig. 2f).

We further compared the chlorination and peroxidase activities of MPO with those of lactoperoxidase (LPO). Luminescence from the LPO assay was substantially lower than that from the MPO assay (Fig. 2g). In the presence of sodium chloride, the LPO reaction produced only 30% of the luminescent signals as compared to the MPO reaction.

Luminol-R-mediated luminescence is dependent on MPO activity

We examined the effect of MPO inhibition on Luminol-R-mediated luminescent light emission under both *in vitro* and *in vivo* conditions. An inhibition assay with the irreversible MPO inhibitor 4-ABAH showed that 4-ABAH dose-dependently inhibited MPO activity at 0–1,500 nM with a half-maximal inhibitory concentration (IC_{50}) of 41 nM (Fig. 3a,b). At high concentrations (>1,000 nM), 4-ABAH inhibited more than 90% of the MPO activity. Under *in vivo* conditions, we found that pretreatment with 4-ABAH attenuated Luminol-R-mediated luminescence in the lungs (Fig. 3c). Quantification of luminescent signals showed that 4-ABAH treatment before LPS administration suppressed the LPS-induced pulmonary MPO activity by 74% (Fig. 3d). This inhibition was statistically significant ($P < 0.05$). Analysis of the lung tissue homogenate showed that 4-ABAH-treated lungs had reduced

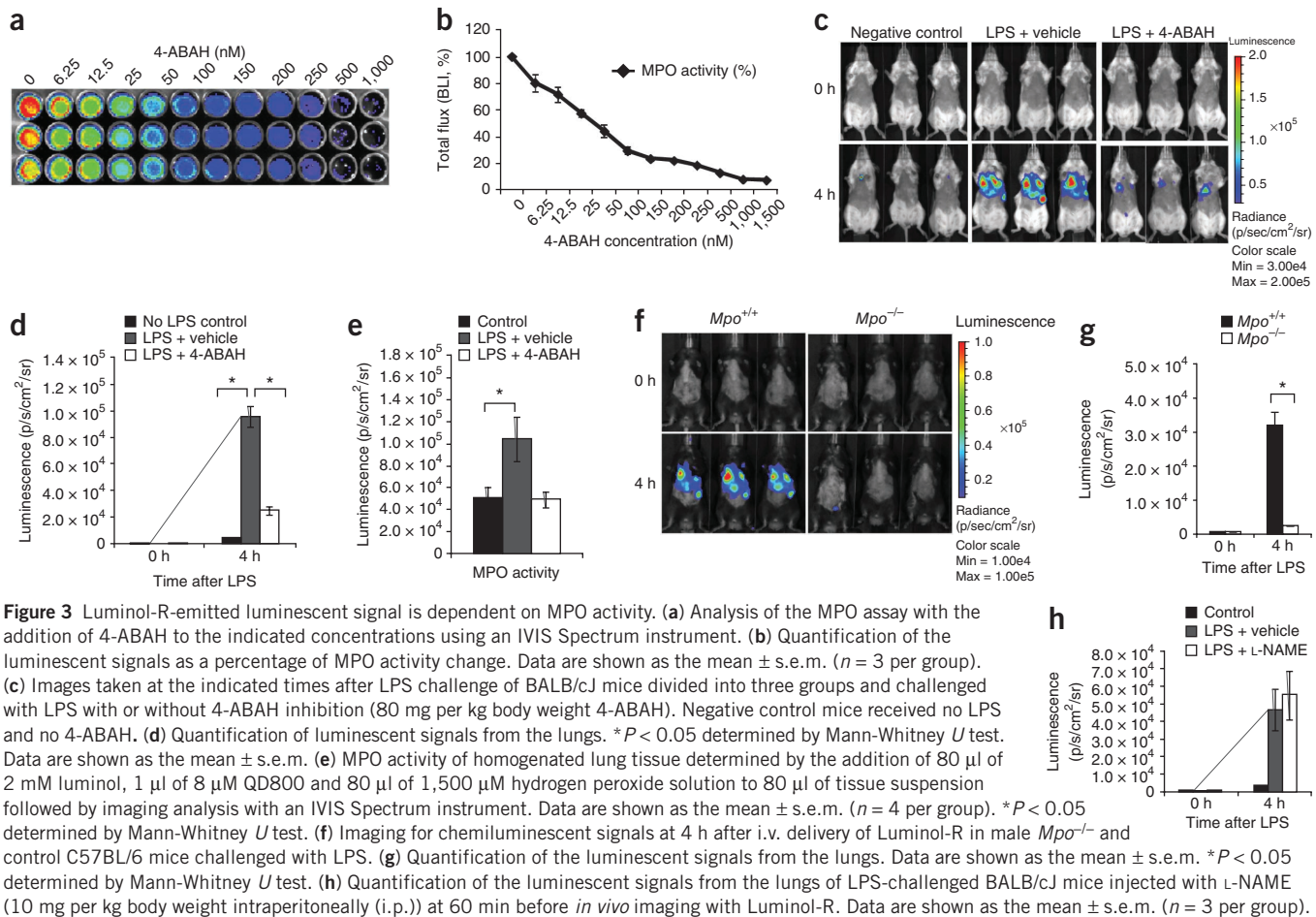
MPO enzymatic activity compared to LPS-treated positive controls (Fig. 3e), verifying that the inhibition was irreversible.

The dependence of the Luminol-R-mediated luminescent signal on MPO activity was further supported in an experiment with MPO-deficient mice. In syngeneic wild-type C57BL/6 (*Mpo*^{+/+}) mice, intratracheal LPS challenge remarkably induced MPO activity in the lungs. In contrast, the MPO activity was significantly ($P < 0.05$) less in LPS-challenged *Mpo*^{-/-} mice (Fig. 3f,g). We then investigated the possible role of nitric oxide on luminescence production. Pretreatment with a nonspecific nitric oxide synthase inhibitor, L-NAME, had no impact on the luminescent signal in the lungs of LPS-challenged mice (Fig. 3h).

Effect of MLN120B on MPO induction

We previously showed that LPS-induced lung injury involves nuclear factor κ B (NF- κ B) activation and that this induction can be suppressed by MLN120B¹². Here we investigated whether inhibition of the NF- κ B signaling pathway by MLN120B affects MPO activity and hypochlorous acid production during pulmonary inflammation. We pretreated mice with MLN120B (300 mg per kg body weight) and then challenged them intratracheally with LPS. Imaging analysis showed that MLN120B pretreatment markedly attenuated the luminescent signal in the lungs as compared to LPS-treated positive control mice (Fig. 4a). The inhibition was as much as 70% (Fig. 4b) and was statistically significant ($P < 0.01$).

We then immunohistochemically analyzed the lung tissues to check whether the inhibition by MLN120B was acting on neutrophil infiltration or inhibition of MPO. Using a neutrophil-specific antibody, Ly-6G, we observed noticeable neutrophil infiltration in LPS-treated lung tissues compared to untreated lungs. MLN120B treatment significantly reduced the infiltration of neutrophils to the lung tissues, resulting in a decrease in MPO activity (Fig. 4c). These results provide evidence of that the NF- κ B signaling pathway is crucial in regulating pulmonary inflammation and MPO production.



Detection of MPO activity from tumor metastases

It has been shown that some malignant tumors attract neutrophil infiltration during their progression¹³. We investigated whether we could use Luminol-R to detect MPO activity in deep tissue tumor metastases. We established systemic MDA-MB-231-luc2 tumor metastasis through intracardiac injection of tumor cells into NU/NU mice. Bioluminescent imaging of the mice, enabled using the *luc*

luciferase gene engineered into these tumor cells, showed the development of multiple metastases on the limbs and mandible and inside the abdominal cavity at 3 weeks after tumor-cell injection (Fig. 5a). At the sites of tumor metastases, in close proximity to the humerus, tibia and femur, osteolytic lesions were evident by micro-computed tomography (microCT) imaging (Fig. 5b–d). After i.v. delivery of Luminol-R to the mice, we were able to detect luminescent signals at all of the

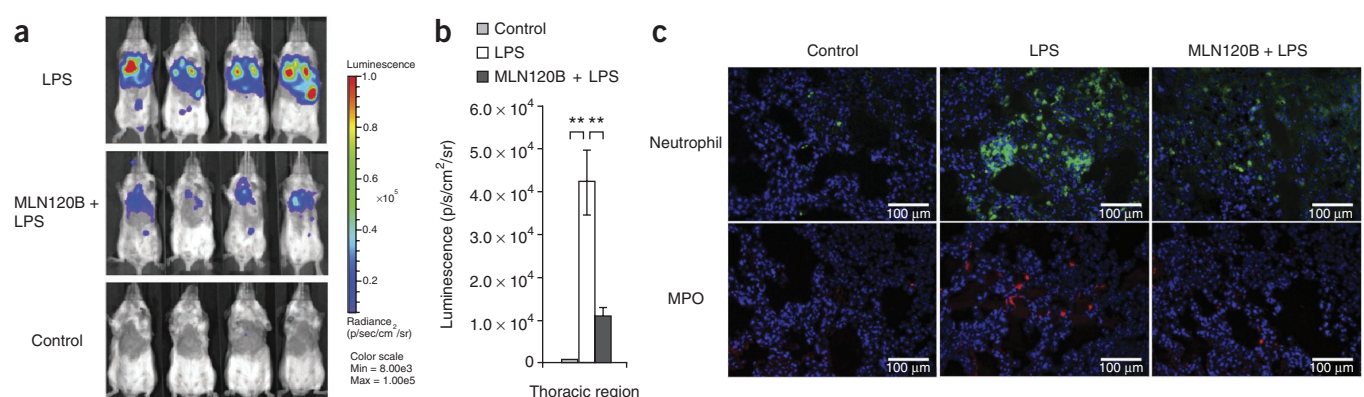
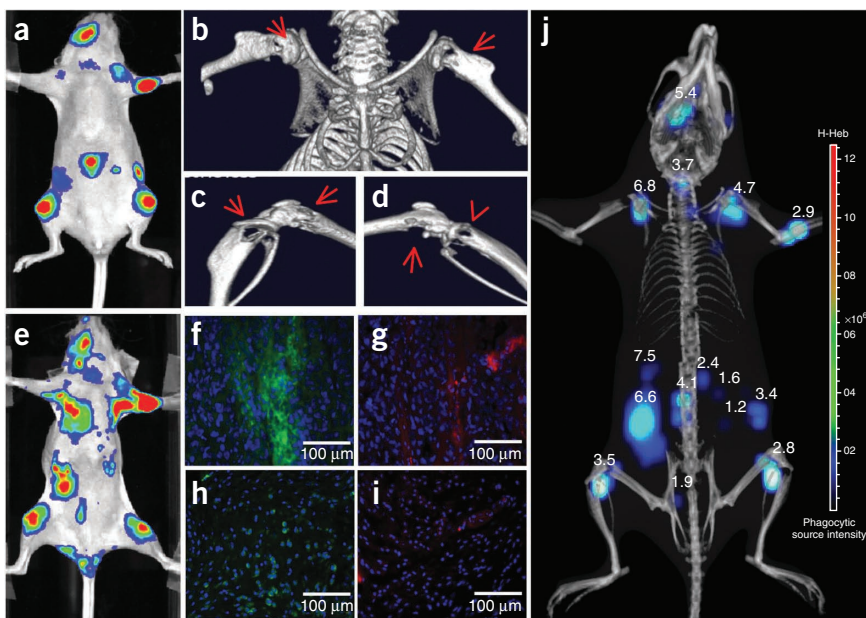


Figure 4 Effect of MLN120B treatment on MPO activity. (a) Induction of MPO activity monitored with Luminol-R in BALB/cJ mice divided into three groups and dosed with MLN120B (300 mg per kg body weight orally) or control vehicle before intra-tracheal LPS challenge. Negative control mice received no LPS and no MLN120B. (b) Quantification of the luminescent signals from the lungs. Data are shown as the mean \pm s.e.m. ($n = 4$ per group). *** $P < 0.01$ determined by Mann-Whitney U test. (c) Fluorescence microscopy performed with a Nuance multispectral charge-coupled device (CCD) camera to visualize neutrophils (green) and MPO (red) in the lung tissues. Nuclei were stained with DAPI (blue). Original magnification, $\times 40$.

Figure 5 Imaging MPO activity in MDA-MB-231-luc2 tumor metastases. (a) Bioluminescent imaging visualizing tumor metastases at 3 weeks in NU/NU mice intracardially injected with MDA-MB-321-luc2 tumor cells. (b–d) High-magnification microCT images obtained using a Quantum FX μ CT system of the shoulders and knee joints showing osteolytic lesions caused by tumor metastases. Arrows indicate regions of osteolytic lesions. (e) MPO activity in these lesions analyzed with Luminol-R. (f–i) Immunohistological analysis of the tumor metastases (f,g) or healthy tissues from a similar area in a control mouse (h,i) analyzed for neutrophils (green; f,h) and MPO (red; g,i) with a Nuance multispectral CCD camera. Nuclei are shown in blue. Original magnification, $\times 40$. (j) Co-registration of multimodality three-dimensional bioluminescent and microCT images obtained using an IVIS Spectrum instrument and a Quantum FX μ CT system, respectively. The DLIT-measured depth (mm) of the tumor metastases is shown above each of the metastatic nodules.



metastatic foci (Fig. 5e), indicating the presence of MPO activity in these lesions. Immunohistochemical analysis showed increased staining of neutrophils and MPO in MDA-MB-231-luc2 tumor metastases (Fig. 5f,g) as compared with healthy tissues from control NU/NU mice in the same anatomical locations (Fig. 5h,i).

We further performed three-dimensional bioluminescent imaging of the mice and estimated the depth of each metastatic lesion with a reconstruction algorithm (DLIT) program. We co-registered the three-dimensional bioluminescent images with three-dimensional microCT images to display all metastatic lesions in a referenced anatomical setting (Fig. 5j). The measured tumor depths ranged from 1.2 mm to 6.8 mm, confirming that Luminol-R-mediated CRET is suitable for monitoring MPO in deep tissue inflammatory foci.

DISCUSSION

Our nanoparticle-based luminescent detection approach relies on a similar energy transfer mechanism as do BRET and CRET, which use conjugation of luminescent enzymes to quantum dots, allowing luminescence to be absorbed and re-emitted by the nanoparticles at a longer wavelength. Recently, fluorescent nanoparticles such as quantum dots have been used as *in vivo* imaging agents because of their broad absorption spectra, high quantum yields and photostabilities^{14,15}. Their blue-increasing extinction coefficient allows fluorescent nanoparticles to be excited more efficiently by shorter-wavelength blue light¹⁶, such as that emitted by luminol, with re-emission of this light in the NIR range. The major finding in this study is that nanoparticles in a nonconjugated form can also effectively convert luminescence to NIR photons. By enabling this photo shift, our nanoparticle-based luminescent detection method allows *in vivo* assaying of endogenous enzymes such as MPO.

Chronic exposure to large amounts of LPS is reported to be associated with the development and progression of many types of pulmonary diseases, including asthma and COPD¹⁷. The pathogenesis of COPD is characterized by neutrophil infiltration of pulmonary tissues and elevated concentrations of MPO in bronchoalveolar lavage fluids¹⁸. MPO is the only enzyme in the body that is known to produce hypochlorous acid, which oxidizes lipids, proteins and DNA^{3,4}.

Hypochlorous acid can be detected with luminol because of the light-emitting reaction of these two components. However, the short wavelength of luminol-emitted luminescence limits its application for the detection of deep tissue MPO activity. Using an LPS-induced lung injury model, we demonstrated that quantum dots were able to convert luminol-emitted blue light to NIR photons that were capable of penetrating tissue at depth. Although the efficiency of energy conversion was only ~13%, the detectability of MPO activity in the lung tissues was improved by 37-fold in Luminol-R-injected mice compared to luminol-injected mice. Our study demonstrated that conversion to NIR luminescence is the unequivocal factor for sensitive MPO detection *in vivo*. MPO production in the lungs during LPS-induced injury correlated with neutrophil infiltration in the lung tissues. In addition, we found direct evidence of elevated amounts of MPO protein in the lung tissues. Using *Mpo*^{-/-} mice, we demonstrated that the Luminol-R-mediated luminescent signal is dependent on MPO activity. We also ruled out any involvement of nitric oxide in luminescence generation using L-NAME, a nonspecific nitric oxide synthase inhibitor¹⁹. We then investigated the ability of Luminol-R to monitor the pharmacological inhibition of MPO. 4-ABAH is the most potent MPO inhibitor that functions as a suicide MPO substrate⁶. We demonstrated that 4-ABAH pretreatment significantly attenuated MPO activity in the lungs.

MPO gene expression is under the regulation of a number of transcription factors, including myeloid nuclear factors 1 α and 1 β ²⁰ and granulocyte colony-stimulating factor¹³. However, there is no evidence of direct involvement of NF- κ B in MPO gene regulation. Nevertheless, evidence showed that under inflammatory disease conditions, NF- κ B activation is accompanied by an elevation of MPO activity in inflamed tissues. In a previous study of LPS-induced lung injury in Sprague-Dawley rats, pulmonary tissues showed NF- κ B activation and elevation of MPO activity²¹. Treatment with penehyclidine hydrochloride resulted in inhibition of the NF- κ B pathway, reduction of MPO activity and suppression of inflammatory cell infiltration to the lung tissues. An increase in MPO activity has also been observed under other disease conditions, such as colitis²². These studies demonstrated that inhibition of NF- κ B activation is associated with

the amelioration of disease symptoms and an attenuation of MPO activity. Our previous study demonstrated that MLN120B suppressed NF- κ B activation during LPS-induced lung injury¹². MLN120B is a potent and selective small-molecule inhibitor of IKK-2 (ref. 23). Here we found that pretreatment with MLN120B attenuated neutrophil infiltration to the lung tissues. MPO comprises between 2% and 5% of the total cellular protein and is the most abundant protein in neutrophils²⁴. Human monocytes also contain MPO-positive granules. However, they are fewer in number than neutrophils. In addition, MPO expression is lost during differentiation into tissue macrophages²⁵. Thus, a substantial contribution of monocytes, macrophages or both to MPO activity during lung injury is unlikely.

Previous studies have shown that most malignant tumors contain a substantial number of leukocytic infiltrates that are linked to poor patient prognosis, with increasing evidence showing that neutrophils actively participate in this process²⁶. Using a systemic MDA-MB-231-luc2 metastatic model, we showed that Luminol-R successfully visualized tumor metastases of various depths, thus establishing that the nanoparticle-based luminescent detection approach can be used to assess MPO activity in lesions beyond superficial levels. In addition to monitoring pulmonary inflammation and the activity of neutrophils in oncogenesis, it is possible that Luminol-R could be used for the diagnostic detection of other neutrophil-associated inflammatory conditions, such as atherosclerosis, peritonitis, arthritis and sepsis. Clinical application of the nanoparticle-based MPO detection method may become possible if Luminol-R is proven safe for use in humans. Of the two agents used in the Luminol-R formulation, luminol has been used to treat humans with alopecia areata²⁷. It can be rapidly cleared from the system without causing toxicity²⁸. The development of fluorescent quantum dots for preclinical and clinical applications involves safety considerations. In preclinical tumor-targeting studies, there have been no observations of short-term toxicity of cadmium-containing quantum dots in mice^{29,30}. The long-term toxicity of these particles to both animals and humans remains unknown. Nevertheless, concerns regarding cadmium toxicity have led to the recent development of cadmium-free quantum dots³¹ and gold-based nanomaterials³². The prospect of applying the nanoparticle-based luminescent detection method in the clinic may draw more research to this area.

METHODS

Methods and any associated references are available in the online version of the paper.

ACKNOWLEDGMENTS

We thank H. Xu for spectrometer analysis, E. Lim and K. Wong for technical assistance and S. Ray and R. Singh for valuable discussion.

AUTHOR CONTRIBUTIONS

Experimental design and concepts were devised by N.Z. and K.P.F., D.A. conducted all the experiments except the *Mpo*^{-/-} study, which was performed by D.A., A.P. and K.P.F., D.A. and N.Z. performed the data analysis. N.Z. wrote the manuscript.

COMPETING FINANCIAL INTERESTS

The authors declare no competing financial interests.

Reprints and permissions information is available online at <http://www.nature.com/reprints/index.html>.

- Haegens, A., Vernooy, J.H., Heeringa, P., Mossman, B.T. & Wouters, E.F. Myeloperoxidase modulates lung epithelial responses to pro-inflammatory agents. *Eur. Respir. J.* **31**, 252–260 (2008).
- Winterbourn, C.C. Reconciling the chemistry and biology of reactive oxygen species. *Nat. Chem. Biol.* **4**, 278–286 (2008).
- Davies, M.J., Hawkins, C.L., Pattison, D.I. & Rees, M.D. Mammalian heme peroxidases: from molecular mechanisms to health implications. *Antioxid. Redox Signal.* **10**, 1199–1234 (2008).
- O'Donnell, C. *et al.* 3-chlorotyrosine in sputum of COPD patients: relationship with airway inflammation. *COPD* **7**, 411–417 (2010).
- Hazen, S.L. & Heinecke, J.W. 3-chlorotyrosine, a specific marker of myeloperoxidase-catalyzed oxidation, is markedly elevated in low density lipoprotein isolated from human atherosclerotic intima. *J. Clin. Invest.* **99**, 2075–2081 (1997).
- Malle, E., Furtmüller, P.G., Sattler, W. & Obinger, C. Myeloperoxidase: a target for new drug development? *Br. J. Pharmacol.* **152**, 838–854 (2007).
- Kettle, A.J., Gedye, C.A. & Winterbourn, C.C. Mechanism of inactivation of myeloperoxidase by 4-aminobenzoic acid hydrazide. *Biochem. J.* **321**, 503–508 (1997).
- Gross, S. *et al.* Bioluminescence imaging of myeloperoxidase activity *in vivo*. *Nat. Med.* **15**, 455–461 (2009).
- Altinoğlu, E.I. & Adair, J.H. Near infrared imaging with nanoparticles. *Wiley Interdiscip. Rev. Nanomed. Nanobiotechnol.* **2**, 461–477 (2010).
- So, M.-K., Xu, C., Loening, A.M., Gambhir, S.S. & Rao, J. Self-illuminating quantum dot conjugates for *in vivo* imaging. *Nat. Biotechnol.* **24**, 339–343 (2006).
- Wang, H.Q. *et al.* Influence of quantum dot's quantum yield to chemiluminescent resonance energy transfer. *Anal. Chim. Acta* **610**, 68–73 (2008).
- Ansaldi, D. *et al.* Imaging pulmonary NF- κ B activation and therapeutic effects of MLN120B and TDZD-8. *PLoS ONE* **6**, e25093 (2011).
- Orita, T., Shimozaki, K., Murakami, H. & Nagata, S. Binding of NF-Y transcription factor to one of the *cis*-elements in the myeloperoxidase gene promoter that responds to granulocyte colony-stimulating factor. *J. Biol. Chem.* **272**, 23216–23223 (1997).
- Wu, X. *et al.* Immunofluorescent labeling of cancer marker Her2 and other cellular targets with semiconductor quantum dots. *Nat. Biotechnol.* **21**, 41–46 (2003).
- Medintz, I.L., Uyeda, H.T., Goldman, E.R. & Mattoussi, H. Quantum dot bioconjugates for imaging, labeling and sensing. *Nat. Mater.* **4**, 435–446 (2005).
- Chan, W.C. & Nie, S. Quantum dot bioconjugates for ultrasensitive nonisotopic detection. *Science* **281**, 2016–2018 (1998).
- Michel, O. *et al.* Severity of asthma is related to endotoxin in house dust. *Am. J. Respir. Crit. Care Med.* **154**, 1641–1646 (1996).
- Linden, M. *et al.* Airway inflammation in smokers with nonobstructive and obstructive chronic bronchitis. *Am. Rev. Respir. Dis.* **148**, 1226–1232 (1993).
- Homayoun, H., Khavandgar, S. & Dehpour, A.R. The involvement of endogenous opioids and nitric oxideergic pathway in the anticonvulsant effects of foot-shock stress in mice. *Epilepsy Res.* **49**, 131–142 (2002).
- Nuchprayoon, I. *et al.* PEBP2/CBF, the murine homolog of the human myeloid AML1 and PEBP2 β /CBF β proto-oncogene, regulates the murine myeloperoxidase and neutrophil elastase genes in immature myeloid cells. *Mol. Cell Biol.* **14**, 5558–5568 (1994).
- Shen, W., Gan, J., Xu, S., Jiang, G. & Wu, H. Penehydridine hydrochloride attenuates LPS-induced acute lung injury involvement of NF- κ B pathway. *Pharmacol. Res.* **60**, 296–302 (2009).
- Islam, M.S. *et al.* Anti-inflammatory effects of phytosterol ferulates in colitis induced by dextran sulphate sodium in mice. *Br. J. Pharmacol.* **154**, 812–824 (2008).
- Nagashima, K. *et al.* Rapid TNFR1-dependent lymphocyte depletion *in vivo* with a selective chemical inhibitor of IKK β . *Blood* **107**, 4266–4273 (2006).
- Schultz, J. & Kaminker, K. Myeloperoxidase of the leucocyte of normal human blood. I. Content and localization. *Arch. Biochem. Biophys.* **96**, 465–467 (1962).
- Bos, A., Wever, R. & Roos, D. Characterization and quantification of the peroxidase in human monocytes. *Biochim. Biophys. Acta* **525**, 37–44 (1978).
- Gregory, A.D. & Houghton, A.M. Tumor-associated neutrophils: new targets for cancer therapy. *Cancer Res.* **71**, 2411–2416 (2011).
- Irie, S. The treatment of alopecia areata with 3-aminophthal-hydrazide. *Curr. Ther. Res. Clin. Exp.* **2**, 107–110 (1960).
- Sanders, J.M., Chen, L.J., Burka, L.T. & Matthews, H.B. Metabolism and disposition of luminol in the rat. *Xenobiotica* **30**, 263–272 (2000).
- Larson, D.R. *et al.* Water-soluble quantum dots for multiphoton fluorescence imaging *in vivo*. *Science* **300**, 1434–1436 (2003).
- Stroh, M. *et al.* Quantum dots spectrally distinguish multiple species within the tumor milieu *in vivo*. *Nat. Med.* **11**, 678–682 (2005).
- Gao, J. *et al.* *In vivo* tumor-targeted fluorescence imaging using near-infrared non-cadmium quantum dots. *Bioconjug. Chem.* **21**, 604–609 (2010).
- Hahn, M.A., Singh, A.K., Sharma, P., Brown, S.C. & Moudgil, B.M. Nanoparticles as contrast agents for *in-vivo* bioimaging: current status and future perspectives. *Anal. Bioanal. Chem.* **399**, 3–27 (2011).

ONLINE METHODS

Reagents. We obtained bacterial LPS, (from *Salmonella abortus-equi*), 4-ABAH, L-NAME and LPO from Sigma-Aldrich Chemical Co. (St. Louis, MO), luminol from Biosynth Chemistry & Biology (Itasca, Illinois), QD800 from Life Sciences (Grand Island, NY) and mouse MPO from R&D Systems (Minneapolis, MN).

Animals. We obtained 8- to 10-week-old female BALB/cJ, C57BL/6 and *Mpo*^{-/-} mice from the Jackson Laboratory (Bar Harbor, Maine) and 8- to 10-week-old female NU/NU mice from Charles River (Wilmington, MA). All animal studies were approved by the Institutional Animal Care and Use Committee at Caliper, Alameda, CA.

Imaging analysis of MPO activity. Acute lung injury was elicited with intratracheal delivery of 50 µl of 10 mg/ml LPS solution to BALB/cJ mice using a 22-gauge intubator. After 3–4 h, mice were i.v. injected with 125 µl of luminol (40 mg/ml) or 137.5 µl of Luminol-R (125 µl of 40 mg/ml luminol mixed with 12.5 µl QD800 (100 pmol)) and imaged in an IVIS Spectrum instrument (Caliper, Alameda, CA) for 5 min with an open filter.

Three-dimensional bioluminescence imaging and µCT co-registration. Mice were i.p. injected with 150 mg per kg body weight luciferin, anesthetized and imaged with narrowband light emission filters (580–640 nm). After optical imaging, the mice were imaged with a Quantum FX µCT system. Three-dimensional reconstruction of the optical and µCT images and co-registration of the two were performed with the Living Image4.2 Software.

In vitro MPO assay with Luminol-R. In a 96-well black plate, an MPO activity assay was set up as follows: 80 µl of 0.5 µg/ml MPO in 150 mM NaCl (pH 7.4) was added to each well and then 80 µl of 2 mM luminol and 1 µl of 8 µM QD800 were added. Eighty microliters of 150 µM hydrogen peroxide solution was added to initiate the reaction. The plate was immediately assayed with an IVIS Spectrum instrument with a 5-min exposure time. In another experiment, the reaction mixture was set up with either 2 nM of LPO or 2 nM of MPO in a final volume of 240 µl. The reactions were assayed as described above. To study the effect of MPO inhibition by 4-ABAH, 10 µl of the 4-ABAH stock solutions were added to the reaction mix before the addition of hydrogen peroxide to obtain final 4-ABAH concentrations of 0, 6.25, 12.5, 25, 50, 100, 150, 200, 250, 500, 1,000 and 1,500 nM. Luminescent signals from each well were quantified using the Living Image software.

Analysis of CRET by spectrometry. In a 1.5-ml ependorff tube, 500 µl of MPO solution (0.6 µM in 150 mM NaCl, pH 7.4) was mixed with 500 µl

of luminol (2,000 µM) and various quantities of 800-nm-emitting quantum dots to achieve final concentrations of 0, 0.05, 0.2 and 0.8 µM. Then 500 µl of hydrogen peroxide solution (2,000 µM) was added to the reaction mix, and the samples were analyzed with a TRIAX 320 spectrometer (Jobin Yvon Instruments, NJ). Freshly resected lung tissues from Luminol-R-injected mice were also applied to spectral analysis with the TRIAX 320 spectrometer.

Dependence of Luminol-R-mediated luminescence on MPO activity. To test the effect of MPO inhibition on Luminol-R-mediated light emission, the MPO inhibitor 4-ABAH (80 mg per kg body weight i.p.) was injected into LPS-challenged BALB/cJ mice 15 min before *in vivo* imaging with Luminol-R. The effect of nitric oxide inhibition was studied by co-treating the LPS-challenged mice with L-NAME (10 mg per kg body weight i.p.) at 60 min before *in vivo* imaging. To study the effect of NF-κB pathway inhibition on LPS-induced luminescent signals, BALB/cJ mice were pre-dosed with MLN120B (in 0.5% methylcellulose, 300 mg per kg body weight orally) at 16 h and 1 h before LPS challenge. Mice were applied to imaging analysis after i.v. injection of Luminol-R. To study the impact of MPO deficiency on Luminol-R-detected luminescence, 8-week-old male *Mpo*^{-/-} mice were challenged with LPS, as above, and applied to imaging detection of the chemiluminescent signal after i.v. delivery of Luminol-R. Age-matched C57BL/6 control mice were used for comparison.

Histology and fluorescence microscopy with Nuance. Histological analysis was performed with a Pentachrome staining kit following the manufacturer's instructions (America Master Tech Scientific, Inc., Lodi, CA). Resected lungs were fixed overnight with 4% paraformaldehyde and embedded in paraffin. Consecutive 5-µm-thick sections were prepared and separately stained with a neutrophil-specific antibody, Ly6G-fluorescein isothiocyanate (FITC) (1:100 dilution, BD Pharmingen, San Diego, CA, catalog number 553126, clone number RB6-8C5) and an MPO rabbit polyclonal antibody (1:1,000 dilution, Abcam, Cambridge, MA, catalog number ab45977). A secondary Cy3 donkey rabbit-specific antibody (Jackson ImmunoResearch Laboratories Inc., West Grove, PA, catalog number 711-165-152) was used for visualizing MPO-positive cells. The nuclei were stained with DAPI-containing mounting media (Vector labs, Burlingame, CA). Fluorescence microscopy was performed with a Nuance multispectral CCD camera (Caliper, Hopkinton, MA).

Statistical analyses. Significance between two means was calculated using a two-tailed Mann-Whitney *U* test. *P* < 0.05 was considered significant. Statistical analyses were performed using Prism 5 (GraphPad Software, Inc., La Jolla, CA).